J. Fluid Mech. (1982), *vol.* 114, *pp.* 41–58
Printed in Great Britain

Stability of imploding shocks in the CCW approximation

By JOHN H. GARDNER, DAVID L. BOOK
Laboratory for Computational Physics, Naval Research Laboratory, Washington, D.C. 20375
AND IRA B. BERNSTEIN
Department of Engineering and Applied Sciences, Yale University, Newhaven, Connecticut

(Received 9 September 1980 and in revised form 9 April 1981)

Analytical and computational techniques are developed to investigate the stability of converging shock waves in cylindrical and spherical geometry. The linearized Chester–Chisnell–Whitham (CCW) equations describing the evolution of an arbitrary perturbation about an imploding shock wave in an ideal fluid are solved exactly in the strong-shock limit for a density profile $\rho(r) \sim r^{-q}$. All modes are found to be relatively unstable (i.e. the ratio of perturbation amplitude to shock radius diverges as the latter goes to zero), provided that q is not too large. The nonlinear CCW equations are solved numerically for both moderate and strong shocks. The small-amplitude limit agrees with the analytical results, but some forms of perturbation which are stable at small amplitude become unstable in the nonlinear regime. The results are related to the problem of pellet compression in experiments on inertial confinement fusion.

1. Introduction

One of the critical limitations to achieving high compression in a spherical implosion is the degree of symmetry that can be maintained. This in turn has important implications for target fabrication techniques and for laser or other driver designs, since it establishes the tolerances required in the symmetry of these components.

An important issue for understanding imploding systems is the stability of a converging shock wave. This shock wave might be used, for instance, not only to compress the fuel, but also to provide the heating required to create a central ignition region. The final temperature achieved will depend on how nearly spherical the shock wave remains during the collapse process and the shape of the shock at the time of reflection.

A certain inherent stability of a shock wave results from the well-known fact that a shock wave with a smaller radius of curvature advances faster than one with a larger radius of curvature. Thus, the part of a perturbed shock front that initially lags behind will accelerate more rapidly owing to its smaller radius of curvature and so will tend to catch up with the remainder of the shock wave. However, the perturbation may be unable to overtake the main shock, which is accelerating because of convergence, or it may be overdriven, i.e. the perturbation may overshoot the stable position.

In order to discuss stability, it is necessary to define what is meant by stable (or unstable) behaviour. The usual definition of stability in terms of a growing or decaying mode amplitude does not adequately describe the situation in imploding systems. For example, the amplitude may not tend to zero as fast as the average radius, or the

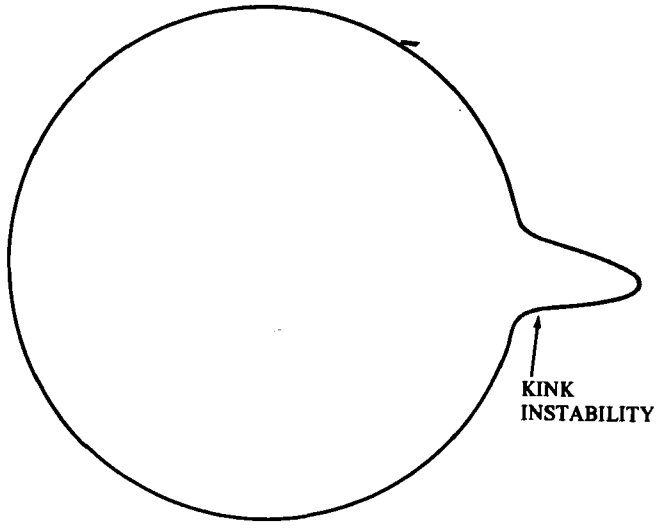

FIGURE 1. Kink instabilities form when the main shock accelerates due to spherical convergence ahead of a perturbed portion of the shock which is unable to catch up in spite of its smaller radius of curvature.

collapse time may be of the order of the period of oscillation of the mode. A more meaningful number for small-amplitude perturbations is the rate of growth (or decay) of the relative perturbation amplitude, i.e. the ratio of the perturbation amplitude to the radius of the zero-order symmetric collapse solution (Bernstein & Book 1978).

Large initial perturbation amplitudes may not decay in the same way as small-amplitude perturbations (Fong & Ahlborn 1979). One can define a radial instability in terms of the maximum deviation of the shock radius from the average radius ($|R-R_{\rm av}|/R_{\rm av}$). Another kind of instability (kink instability) occurs when a small portion of the shock necks off from the central region (figure 1). In general, we cannot speak of an imploding shock as being stable or unstable in a clear-cut sense. Rather, we can ask whether it retains an acceptable degree of symmetry after having collapsed to a volume sufficiently small for practical purposes.

We have developed an analytic and computational model to investigate the stability of converging shock waves in cylindrical and spherical geometry. This represents an extension to smaller radii of the work of Fong & Ahlborn (1979) on the linear stability problem. The model equations are described in the next section, followed by a linearized analytic solution, an account of the numerical model, a comparison of the numerical and analytic solutions, an analysis of nonlinear behaviour, and an extension to problems with a varying density in front of the shock.

2. Model equations

The motion of a converging shock wave can be computed with great accuracy by considering only changes in the physical variables across the shock front, and ignoring the fluid motion behind the shock surface. The velocity of a shock front in a motionless undisturbed medium is normal to the front. It may therefore be treated as a locally one-dimensional motion in a channel whose boundaries are determined by the trajectories

of the shock front. These trajectories form imaginary ray tubes whose cross-sectional area is related to the Mach number by an equation derived by Chester (1954), Chisnell (1955) and Whitham (1957) (the CCW approximation). Butler (1955) made use of a similar technique. The equation may be found by substituting into the compatibility equation for the characteristic moving in the direction of shock propagation the fluid quantities determined by the Rankine–Hugoniot relations across the shock. Whitham (1958) has shown that this procedure, the simplest method of deriving the CCW approximation, is equivalent to solving the complete fluid equations while ignoring the influence of the characteristics which are overtaking the shock from behind. For this reason, it is most accurate for shocks of the self-propagating type where disturbances more than a small distance behind never catch up with the shock, which is generally accelerating (Hayes 1968).

The result of this model is an equation for the Mach number M of the shock as a function of the cross-sectional area A of the ray tube:

$$\frac{\lambda(M)\,M\,dM}{M^2-1}+\frac{dA}{A}=0, \tag{1}$$

where

$$\lambda(M)=\left(2\sigma+1+\frac{1}{M^2}\right)\left(1+\frac{2}{\gamma+1}\frac{1-\sigma^2}{\sigma}\right) \tag{2}$$

and

$$\sigma^2=\frac{(\gamma-1)M^2+2}{2\gamma M^2-(\gamma-1)}, \tag{3}$$

where γ is the usual adiabatic index. The cross-sectional area of the ray tube may be expressed in terms of the shock-front velocity by the kinematic relations

$$\dot{A}=-A\mathbf{n}.(\mathbf{n}\times\nabla)\times\mathbf{v}, \tag{4}$$

$$\dot{\mathbf{n}}=-(\mathbf{I}-\mathbf{nn}).(\mathbf{n}\times\mathbf{v})\times\mathbf{v}, \tag{5}$$

$$\dot{\mathbf{r}}=\mathbf{v}=\mathbf{n}v, \tag{6}$$

where a dot over a variable denotes a derivative with respect to time, $\mathbf{n}$ is the unit vector normal to the shock front and $\mathbf{r}$ is the surface location.

In numerical integration, equations (1) and (5) are used to propagate the magnitude and direction, respectively, of the shock-front velocity in terms of time, substituting $\dot{A}$ from (4). Equation (6) then advances the shock-front position by integration of the velocity. For small perturbations about symmetric (cylindrical or spherical) shocks, however, solutions can be obtained analytically.

3. Linearized analytic solutions

Since all collapsing shocks will eventually become strong, it is useful to analyse the strong shock limit $M\gg 1$. If we assume that the sound speed ahead of the shock is constant, in addition to being small, then (1)–(3) reduce to

$$\dot{A}/A-\lambda\dot{v}/v, \tag{7}$$

where

$$v=M/a, \quad \text{and} \quad \lambda=\frac{\gamma+2}{\gamma}+\left(\frac{2\gamma}{\gamma-1}\right)^{\frac{1}{2}}. \tag{8), (9}$$

Using familiar vector identities, we have

$$\mathbf{n}.(\mathbf{n}\times\nabla)\times\mathbf{v} = -v\nabla.\mathbf{n}. \tag{10}$$

Thus, using (4) and (7)–(10), we have

$$(\lambda/v)^{\cdot} \equiv d/dt(\lambda/v) = \nabla.\mathbf{n} = \mathbf{n}\times(\mathbf{n}\times\nabla).\mathbf{n}, \tag{11}$$

which only involves tangential derivatives of $\mathbf{n}$. We first look at the zeroth-order symmetric solution,

$$\dot{r} = v(t), \quad \mathbf{n} = \mathbf{e}_r, \quad \dot{\mathbf{n}} = 0, \tag{12), (13), (14}$$

$$(\lambda/\dot{r})^{\cdot} = \nabla.(\mathbf{r}/r) = \alpha/r, \tag{15}$$

where $\alpha = 1$ (2) for cylindrical (spherical) geometry. Equations (12)–(15) can be rewritten as

$$\dot{r}\frac{d}{dr}\left(\frac{\lambda}{\dot{r}}\right) = -\lambda\frac{d}{dr}\ln\dot{r} = \frac{\alpha}{r} = \frac{d}{dr}\ln r^{\alpha}. \tag{16}$$

Integrating this once yields

$$\dot{r}r^{\alpha/\lambda} = \text{const.}, \tag{17}$$

and finally

$$r = R(\omega t)^{\lambda/(\lambda+\alpha)}, \tag{18}$$

where R and ω are constants.

Suppose we now linearize the equation by assuming $\mathbf{n} = \mathbf{n}_0+\mathbf{n}_1$, $\mathbf{v} = \mathbf{v}_0+\mathbf{v}_1$, $\mathbf{r} = \mathbf{r}_0+\boldsymbol{\xi}(\mathbf{r}_0, t)$, where the subscript 0 refers to the zeroth-order symmetric solution, and the subscript 1 refers to a small perturbation about this solution. From equation (5) we have

$$\mathbf{n}_1 = -(\mathbf{I}-\mathbf{n}_0\mathbf{n}_0).(\mathbf{n}_0\times\nabla_0)\times\boldsymbol{\xi}. \tag{19}$$

Expanding the gradient operator

$$\nabla = \nabla_0-(\nabla_0\boldsymbol{\xi}).\nabla_0+\ldots, \tag{20}$$

from (11) we have to first order

$$(-\lambda v_1/v_0^2)^{\cdot} = \nabla_0.\mathbf{n}_1-(\nabla_0\boldsymbol{\xi}):(\nabla_0\mathbf{n}_0). \tag{21}$$

From (19) after some manipulation we have

$$\mathbf{n}_1-\boldsymbol{\xi}.\nabla_0\mathbf{n} = -(\mathbf{I}-\mathbf{n}_0\mathbf{n}_0).\nabla_0(\mathbf{n}_0.\boldsymbol{\xi}). \tag{22}$$

Here use has been made of the facts that $\mathbf{n}_0 = \mathbf{e}_r$ and that

$$\nabla_0\mathbf{n}_0 = \nabla_0(\mathbf{r}_0/r_0) = (\mathbf{I}-\mathbf{n}_0\mathbf{n}_0)/r_0 \tag{23}$$

is a symmetric dyad. From equation (6) we have

$$\dot{\boldsymbol{\xi}} = \mathbf{n}_0 v_1+\mathbf{n}_1 v_0. \tag{24}$$

Hence taking the scalar product with $\mathbf{n}_0$ yields

$$\mathbf{n}_0.\dot{\boldsymbol{\xi}} = (\mathbf{n}_0.\boldsymbol{\xi})^{\cdot} = v_1. \tag{25}$$

Thus equation (21) can be written as

$$\begin{aligned}-\left(\frac{\lambda\mathbf{n}_0.\boldsymbol{\xi}}{v_0^2}\right)^{\cdot} &= \nabla_0[\mathbf{n}_1-\boldsymbol{\xi}.\nabla_0\mathbf{n}_0]+\boldsymbol{\xi}.\nabla_0\nabla_0.\mathbf{n}_0\\ &= -\nabla_0.[(\mathbf{I}-\mathbf{n}_0\mathbf{n}_0).\nabla_0(\mathbf{n}_0.\boldsymbol{\xi})]+\boldsymbol{\xi}.\nabla_0\left(\frac{\alpha}{r_0}\right).\end{aligned} \tag{26}$$

Now if we expand the perturbation in either cylindrical or spherical harmonics by assuming a sum of linearly independent terms of the form

$$\mathbf{n}_0 \cdot \boldsymbol{\xi} = \zeta(t) \cos(m\phi) \quad \text{(cylindrical)} \tag{27}$$

$$= \zeta(t) P_l^m(\theta) \cos(m\phi) \quad \text{(spherical)}, \tag{27'}$$

each of which can be treated independently, and define the mode-number-dependent coefficient of the Laplacian by

$$Q = m^2 \qquad \text{(cylindrical)} \tag{28}$$

$$= l(l+1) \quad \text{(spherical)}, \tag{28'}$$

equation (26) becomes

$$-(\lambda \dot{\zeta}/v_0^2)^{\cdot} = \zeta(Q-\alpha)/r_0. \tag{29}$$

Now using

$$\dot{\zeta} = v_0 \frac{d\zeta}{dr_0}, \tag{30}$$

we have

$$v_0 \frac{d}{dr_0}\left[\frac{\lambda}{v_0}\frac{d\zeta}{dr_0}\right] = \frac{\alpha - Q}{r_0^2}\zeta. \tag{31}$$

From equation (18) we have

$$\frac{d \ln v_0}{dr_0} = -\frac{\alpha}{\lambda r_0}, \tag{32}$$

and after a little algebraic manipulation we get

$$\lambda \frac{d^2\zeta}{dr_0^2} + \frac{\alpha}{r_0}\frac{d\zeta}{dr_0} + \frac{Q-\alpha}{r_0^2}\zeta = 0. \tag{33}$$

We now seek a solution of the form $\zeta \sim r_0^\beta$, where β is in general a complex number which satisfies the indicial equation

$$\lambda\beta(\beta-1) + \alpha\beta + Q - \alpha = 0, \tag{34}$$

or

$$\beta = \frac{1}{2\lambda}\{\lambda - \alpha \pm [(\lambda+\alpha)^2 - 4\lambda Q]^{\frac{1}{2}}\}. \tag{35}$$

Since we seek the ratio of the amplitude of the disturbance to that of the zeroth-order solution we look at

$$\zeta/r_0 \sim r_0^{\beta-1} = r_0^{\{-(\lambda+\alpha)\pm[(\lambda+\alpha)^2-4\lambda]^{\frac{1}{2}}\}/2\lambda}. \tag{36}$$

Since

$$r_0 \sim t^{\lambda/(\lambda+\alpha)}, \tag{37}$$

$$\zeta/r_0 \sim t^{-\frac{1}{2}\pm[(\lambda+\alpha)^2-4\lambda Q]^{\frac{1}{2}}/2(\lambda+\alpha)}. \tag{38}$$

Equation (38) is identical with a result obtained by Butler in an unpublished report and quoted in Butler (1955). Whitham (1974) derived an equivalent formula valid for the cylindrical case by a different technique.

For the lowest-order mode numbers $\beta - 1$ is real and negative, indicating that the disturbance is geometrically unstable:

$$\beta - 1 = -\frac{\lambda+\alpha}{\lambda}, 0 \tag{39}$$

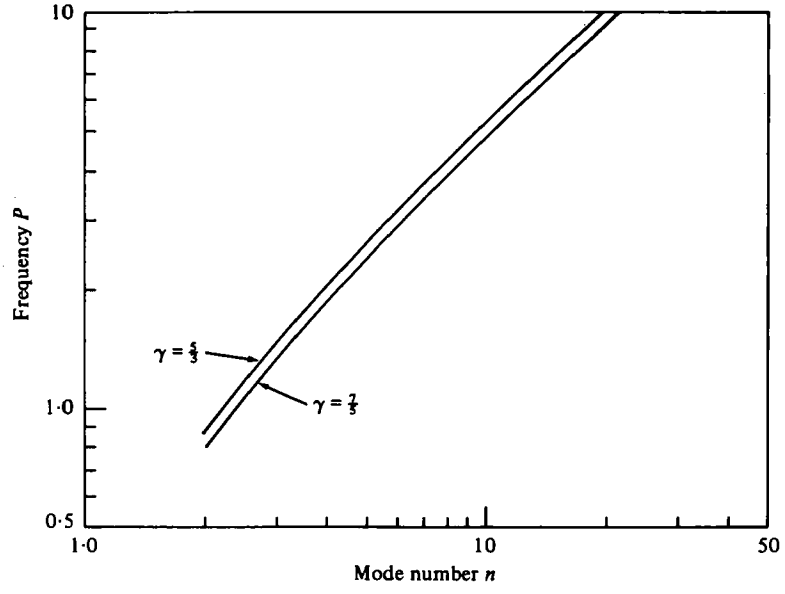

FIGURE 2. Oscillation frequency in $\ln t$ of spherical harmonic perturbation of a spherical shock front as a function of mode number for a perfect gas with $\gamma = \frac{5}{3}$ and $\gamma = \frac{7}{5}$.

for $l = 0$ (spherical co-ordinates) or $m = 0$ (cylindrical co-ordinates), and

$$\beta - 1 = -\frac{\alpha}{\lambda}, -1 \tag{40}$$

for $l = 1$ (spherical co-ordinates) or $m = 1$ (cylindrical co-ordinates). For all mode numbers greater than unity β is complex, and there is a factor growing with a power-law dependence $\sim r^{-(\lambda+\alpha)/(2\lambda)}$ and a factor which is oscillatory in $\ln r_0$ with a frequency $\omega = \frac{1}{2}(4\lambda Q - (\lambda+\alpha)^2]^{\frac{1}{2}}/\lambda$. The real part is always negative and independent of mode number, while the oscillatory part depends on the mode number:

$$\zeta/r_0 \sim r_0^{-(\lambda+\alpha)/2\lambda \pm ip(\lambda+\alpha)/\lambda}, \tag{41}$$

where

$$p = \frac{[4\lambda Q - (\lambda+\alpha)^2]^{\frac{1}{2}}}{2(\lambda+\alpha)}. \tag{42}$$

In figure 2 we show the frequency in $\ln t$ for the spherical harmonic perturbation as a function of mode number for two different ratios of specific heat, $\gamma = \frac{7}{5}$ and $\gamma = \frac{5}{3}$. Figure 3 shows the ratio r/r_0 between successive minima in the perturbation amplitude as it oscillates during collapse. The ratio may be chosen so that at some prescribed degree of compression the perturbation amplitude is a minimum.

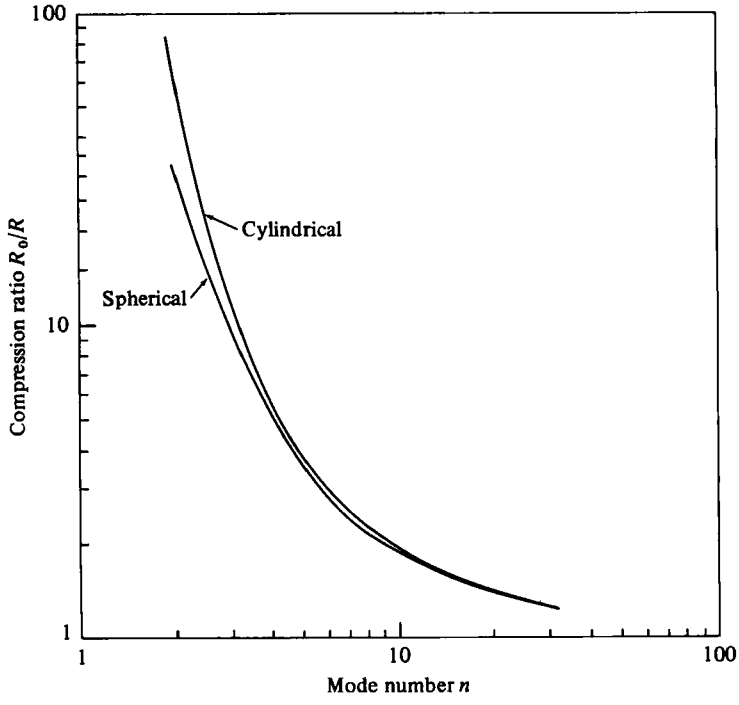

FIGURE 3. Compression ratio between successive minima in perturbation amplitude during perturbed shock collapse as a function of mode number.

4. Numerical integration

In order to assess the importance of nonlinear effects on the mode amplitude, the full nonlinear model equations were integrated with a code similar to that of Fong & Ahlborn (1979). The code advances the equations of motion of the shock front

$$\dot{\mathbf{r}} = \mathbf{v}, \tag{43}$$

$$\frac{dM}{dA} = \frac{M^2-1}{\lambda(M)\,MA}, \tag{44}$$

either in plane co-ordinates (for cylindrical collapse viewed in a plane through the axis) or in cylindrical co-ordinates (for spherical collapse viewed in the equatorial plane).

The equation for the cross-sectional area is not integrated directly, but areas are taken from the kinematics of the integrated ray tubes. A second-order-accurate, space-and-time-centred algorithm is employed to advance the grid locations and Mach numbers. Thus the problem of computing the shock shape is reduced to integrating a set of ordinary differential equations for the trajectories of a finite number of grid points located along the shock front, and for their associated time-dependent Mach numbers. The integration is subject to a timestep limit analogous to the Courant condition for the one-dimensional fluid equations. This algorithm allows for the propagation of so-called shock-shocks (discontinuities in the slope and Mach number of the shocks predicted by the Whitham theory) in either direction, since the scheme is centred and symmetric. The equations for the shock surface are analogous to the one-dimensional Lagrangian equation of motion, where the shock position takes the

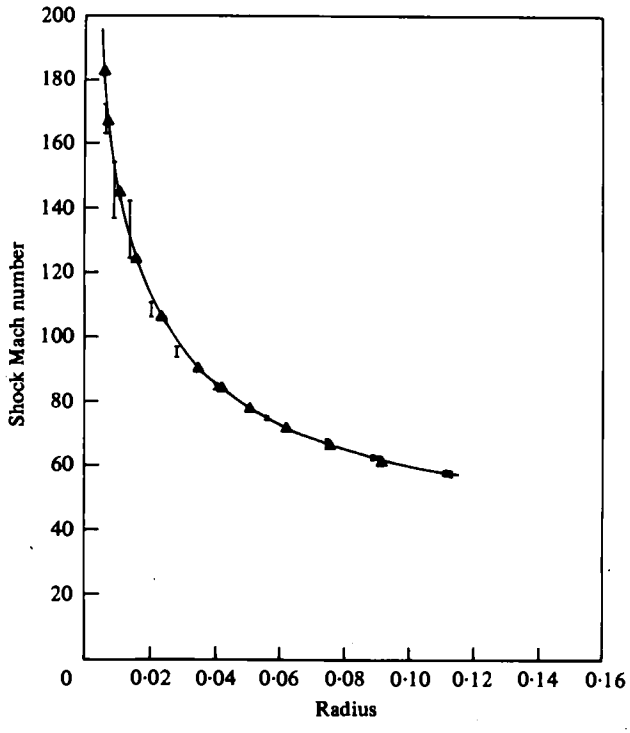

FIGURE 4. Comparison of analytic and numerical integration for self-similar spherical-shock collapse (Guderley problem). I, one-dimensional fluid code; ▲, numerical shock integration; ——, strong-shock similarity solution.

place of the fluid position, the ray tube area takes the place of fluid density, and the Mach number takes the place of the fluid velocity. Thus many of the properties of one-dimensional motion, e.g. disturbances travelling along characteristic directions and nonlinear wave front stepening, show up in the shape of the shock surface.

It was found necessary to redistribute the grid points to prevent unacceptably short timesteps as the mesh points crowd together near the shock-shock regions. The algorithm diffuses the grid points a small amount parallel to the shock front in such a way as to make the distances between points more nearly equal. This diffusion plays a role similar to that of an artificial surface tension at interfaces.

To test the accuracy of the numerical procedure described above, we compared the results of the calculation with those predicted by the self-similar solutions for the collapse of an infinitely strong shock due to Guderley (1942). The self-similar solution predicts a shock position given by $R = C(-t)^{\eta}$ with $\eta = 0{\cdot}717$ for a $\gamma = 1{\cdot}4$ gas according to Guderley. This gives a shock Mach number as a function of radius

$$\dot{R} = -\eta C(-t)^{\eta-1} \sim R^{(\eta-1)/\eta}. \tag{45}$$

Thus

$$M \sim R^{(\eta-1)/\eta} = R^{-0{\cdot}3947}. \tag{46}$$

The CCW approximation for large M gives

$$\frac{dA}{A} = 2\frac{dR}{R} = \left(1+\frac{2}{\gamma+1}\frac{1-\sigma^2}{\sigma}\right)\frac{(2\sigma+1)M^2+1}{M^2-1}\frac{dM}{M} \tag{47}$$

with

$$\sigma = \left[\frac{\gamma-1}{2\gamma}\right]^{\frac{1}{2}}.$$

This yields

$$M \sim R^{-(2\gamma\sigma)/(2\sigma+1)(\gamma\sigma+1)} = R^{-0\cdot3941}. \tag{48}$$

The exponents agree with the analytic Guderley solution to within 0·0006. In figure 4 we show the results of these models for the spherical convergence of a shock with an initial Mach number of 57 at a radius of 0·112 cm. The solid line is the analytic result of the Guderley solution. The triangles are the numerical results of the CCW approximation using the code described above with 25 mesh points around a circle in cylindrical co-ordinates (describing a spherical implosion). Comparing the results along the axis with those perpendicular to the axis, we see that the shock remains spherical to better than 1 % during the entire implosion and the Mach number reproduces the Guderley solution with less than 0·5 % error.

5. Comparison of results of linearized model and nonlinear integration

In figures 5 and 6 we show the results of the analytic and numerical integration for mode numbers 2, 4 and 8 for cylindrical and spherical collapse. The solid lines are the analytic formulae and the circles show the numerical results. To ensure that we begin in the linear regime an initial amplitude of the modes was chosen such that $\zeta/r_0 = 10^{-3}$. Since the system of equations is second order in the perturbed shock location, both the amplitude and the velocity of perturbation must be specified. For these cases the velocity was chosen to be zero. This then uniquely determines the phase of the oscillation. The phase angle between the amplitude and the velocity is determined by the mode number and the specific heat ratios:

$$\phi = \tan^{-1}\left[\frac{\lambda-\alpha}{2(\lambda+\alpha)p}\right]. \tag{49}$$

Agreement appears very good until the mode amplitude becomes greater than a few per cent. At this time nonlinear effects which can generate modes other than primary one drive the solution away from the linear result. Nonlinear steepening of the wave front generates higher-order modes which begin to dominate the solution. In figure 7 we can see the form this takes. This figure shows the successive wave-front shapes for an $l = 8$ spherical harmonic perturbation started with a large amplitude in order to show the effects of a large compression. As the shock collapses, the wave fronts begin to form cusplike-shapes in the region where the shock is left behind. For sufficiently large amplitudes a true cusp forms and the simple shock front no longer exists. It is replaced by a system of reflecting shock waves (see figure 8), which, however, are not treated in the present model. Whether regular or Mach shock reflection occurs depends on whether the angle between the shocks is less or greater than the critical angle ($\simeq 75°$ for $\gamma = 1{\cdot}4$, $M = \infty$). In most cases the angle in the cusp has been less than the critical angle. When this occurs a large portion of the shock energy can be left behind in the reflected shock system, thus decreasing the compressional effect of the imploding shocks. Solutions of this type are referred to below as having kink instabilities in the shock front.

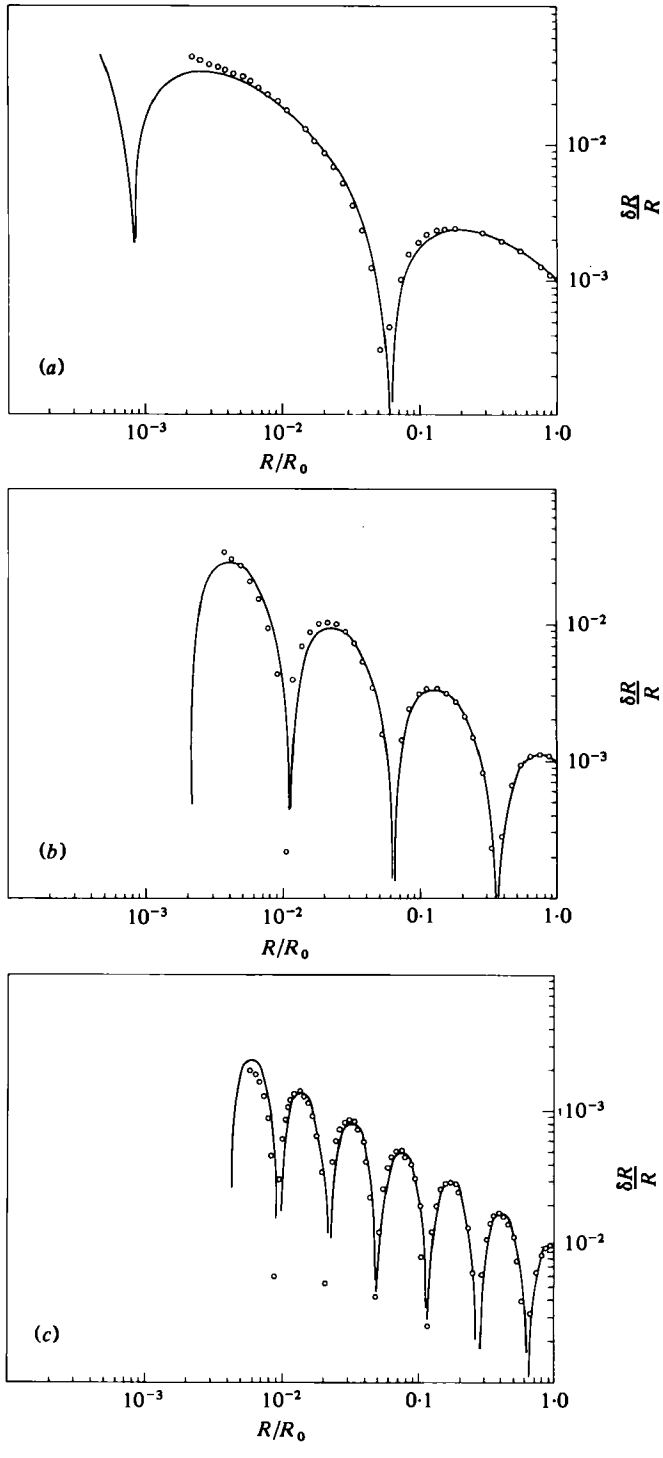

FIGURE 5. Comparison of analytic (solid lines) and numerical (open circles) for maximum perturbation amplitude as a function of radius for cylindrical shock collapse at three different mode numbers: (*a*) $n = 2$; (*b*) $n = 4$; (*c*) $n = 8$. Deviation at small radii is due to nonlinear effects not in analytic model.

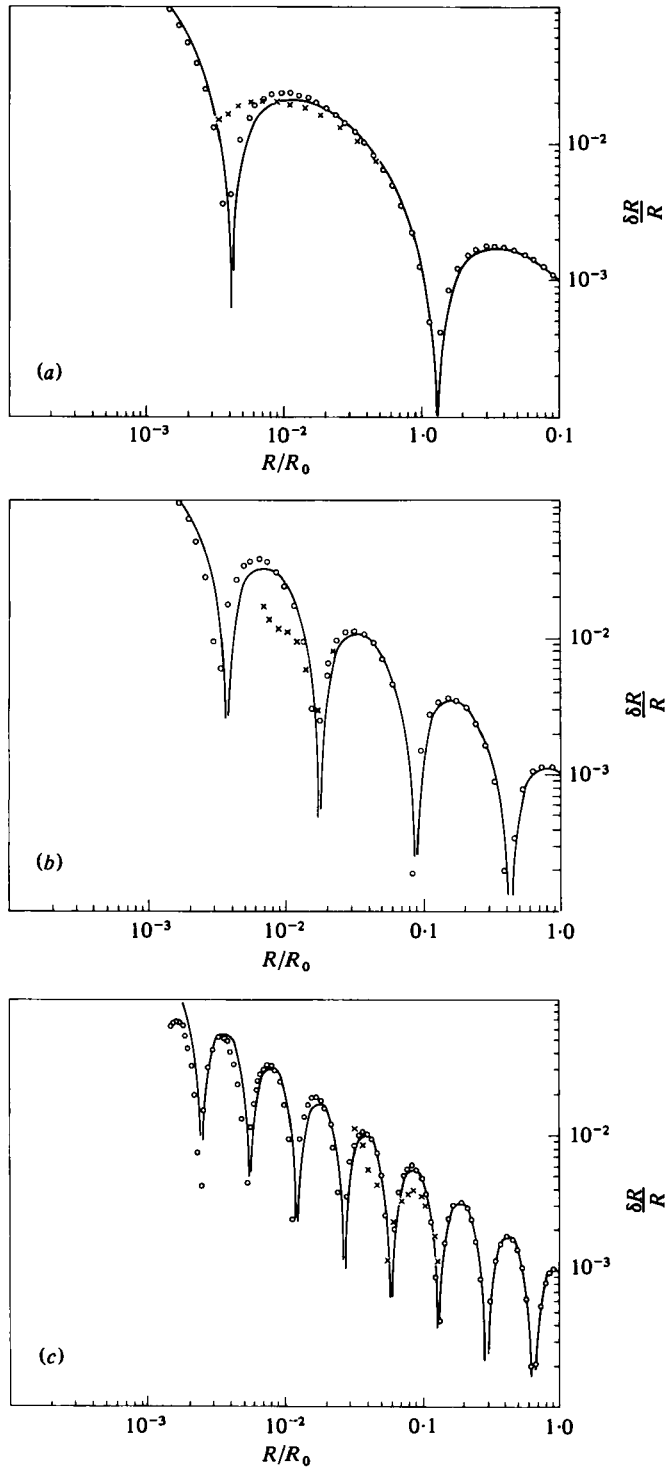

FIGURE 6. Comparison of analytic (solid lines) and numerical results (open circles) for spherical shock collapse for three different mode numbers: (*a*) $n = 2$; (*b*) $n = 4$; (*c*) $n = 8$.

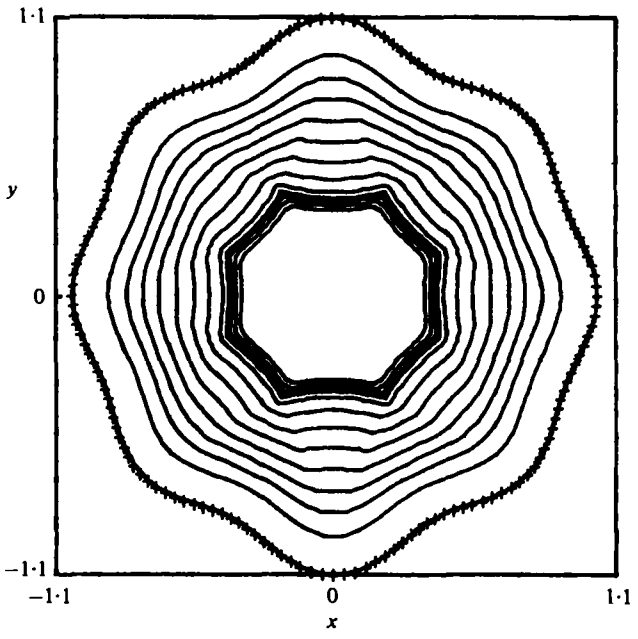

FIGURE 7. An example showing formation of cusp-like structure for large perturbation amplitudes in the nonlinear regime. Initial perturbation is a mode-number-8 Legendre polynomial with amplitude 10 % of mean radius.

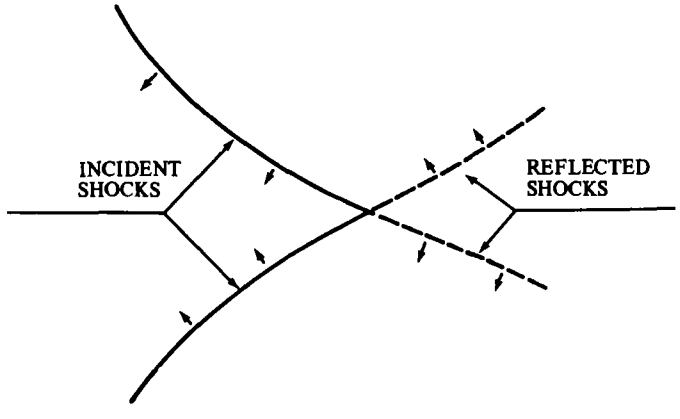

FIGURE 8. In the nonlinear regime shock-shocks are formed which are the intersections of regular or Mach reflections of shocks. This results in potential loss of shock energy in the reflected shock system.

6. Nonlinear modelling

In order to investigate more carefully how these kinks form and propagate, we look at perturbation in the form of a simple spherical cap of radius smaller than the initial mean shock radius. This shock cap intersects the main shock with an angle δ at a colatitude β, as shown in figure 9. For the purpose of this investigation the Mach number around the shock is assumed uniform at $M = 10$. In figure 10 we show the limits of stability for δ as a function of β. In addition we show the stability result in terms of $\delta r_0/r_0$ as a function of β ($\delta r_0/r_0$ is geometrically related to δ and β). When

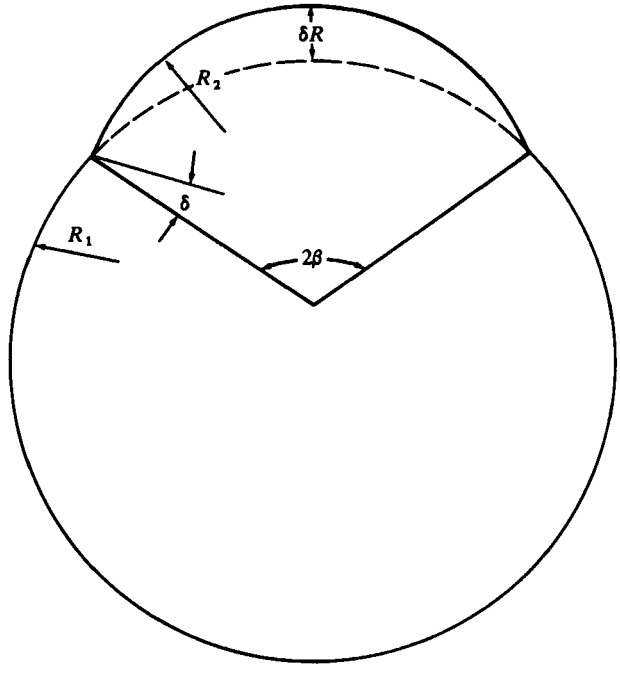

FIGURE 9. Initial perturbation of a spherical shock may be represented in terms of a cap at one pole with a radius of curvature smaller than the main shock. The perturbation magnitude δR, intersection half-angle β, and deviation angle δ are related by geometry.

either δ or β becomes too large, the shock front is transformed into a nonlinear cusp-type regime instead of reverting to a more spherical form and oscillating. From figure 10(*b*) we can see that this is related to the initial perturbation and is a function of β. In each case instability is defined to occur if a cusp shock is formed before $r/r_0 < 10^{-2}$. This arbitrary definition is necessitated by the fact that all perturbations, given sufficient compression, eventually evolve into the cusp-shaped form. Realistically speaking, however, compressions of 10^6 are more than sufficient to achieve the compression and temperature rise necessary for ignition in pellet fusion.

Even for these single cap perturbations, oscillatory behaviour is apparent for sufficiently small initial amplitudes. Let us compare the radius of the first minimum of the average deviation from a spherical or cylindrical shock for the cap perturbation with that for Legendre polynominal whose first zero forms the same angle as the β for the cap perturbation. We see from figure 11 that at least for smaller β (i.e. larger l) the oscillation period is nearly the same. This indicates that the oscillation period (i.e. the time or radius between minimum deviations from symmetric implosion) can be reasonably well predicted for arbitrary perturbations by matching to the lowest-order Legendre polynominal which fits the perturbation. In figure 12 we show a stable case where the behaviour about a nearly spherical implosion is oscillatory up to a compression of $r_0/r = 10$. In figure 13 we show an unstable case where a cusp is clearly forming after a single overshoot of the perturbation and a compression of $r_0/r = 4$.

From these results we see that two interdependent factors control when the nonlinear kinks will begin to form. One is the wavelength of the perturbation and the other is the angle at which the perturbation intersects the mean radius. The smaller the

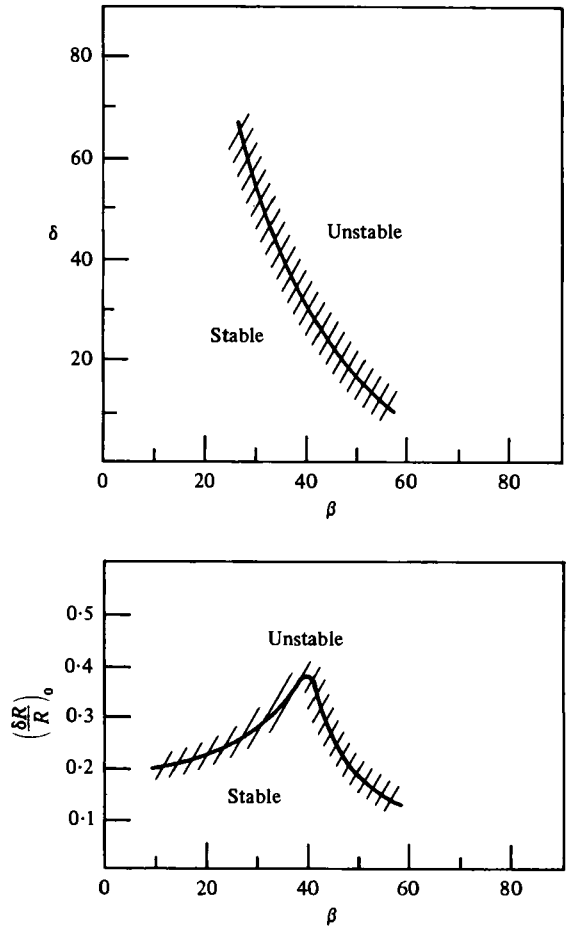

FIGURE 10. (*a*) Stability limits for the spherical cap perturbation are given as a function of the deviation angle δ and intersection angle β as defined in figure 9. Instability is defined to occur when a kink forms before a compression radius $R/R_0 < 0{\cdot}01$. (*b*) Stability limits are shown as a function of $(\delta R/R)_0$ and β. These two graphs are connected by simple geometric relations.

wavelength, the larger the angle that is tolerable. Note, however, that this angle and the mode amplitude are not independent. In terms of amplitude, the shorter the wavelength, the smaller the amplitude of disturbance that can be tolerated.

7. Non-uniform undisturbed density

Equation (1) was derived assuming a uniform density and temperature ahead of the shocks. The CCW methodology does not require the medium ahead of the shocks to be uniform, and we shall now investigate the effect a non-zero density variation in the undisturbed medium of the form $\rho(r) \sim r^{-q}$. However, for the shock to remain of the accelerating, self-propagating type requires $\alpha - \kappa q > 0$, where κ is defined in (54) and (55). While the characteristic exponent has an accuracy generally better than 0·1 % for the imploding shock problem, it is considerably less accurate (5–10 % errors) for the varying density cases (Sakurai 1960). Corrections to the CCW characteristic

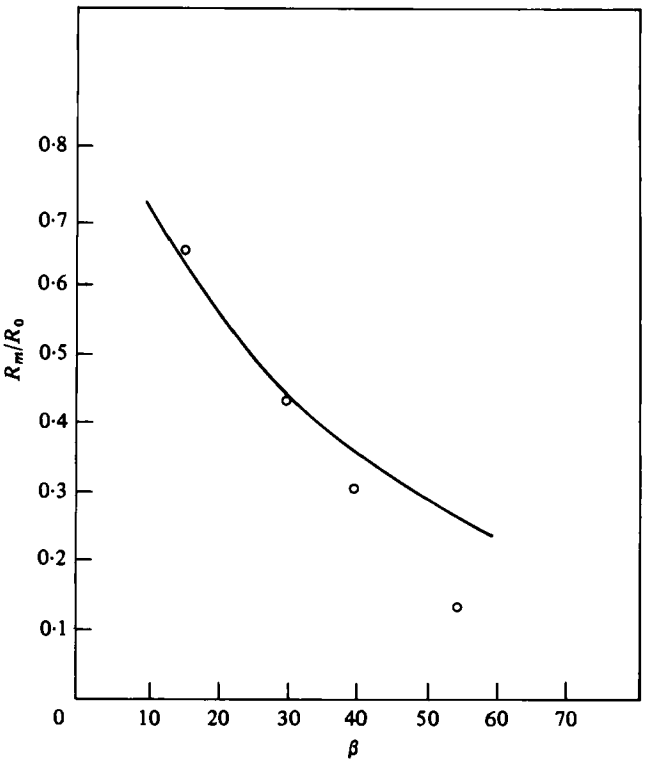

FIGURE 11. Compression ratio at the first minimum of $\delta R/R$ as a function of intersection angle. Open circles represent results obtained with Legendre polynomials, where β is the angle to the first zero.

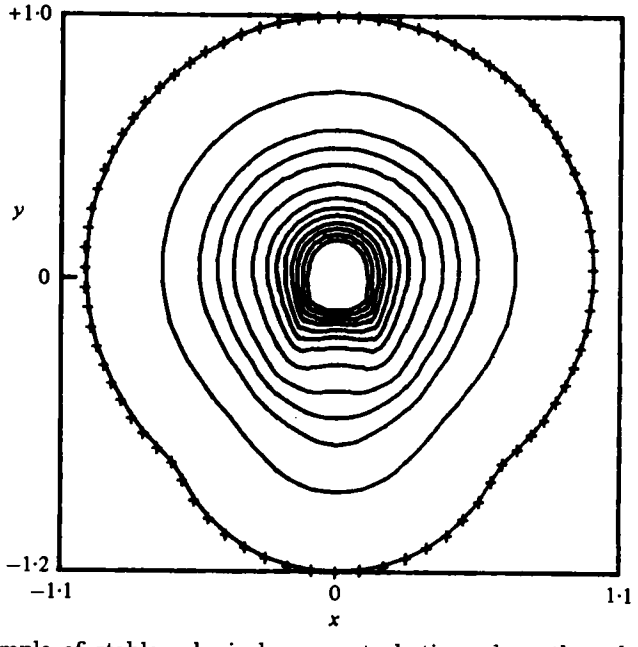

FIGURE 12. Example of stable spherical cap perturbation where the solution oscillates and tends to become more spherical. No kinks appear before $R/R_0 < 0{\cdot}01$. ($\alpha = 29°$, $\beta = 39°$, $\delta R/R = 0{\cdot}2$.)

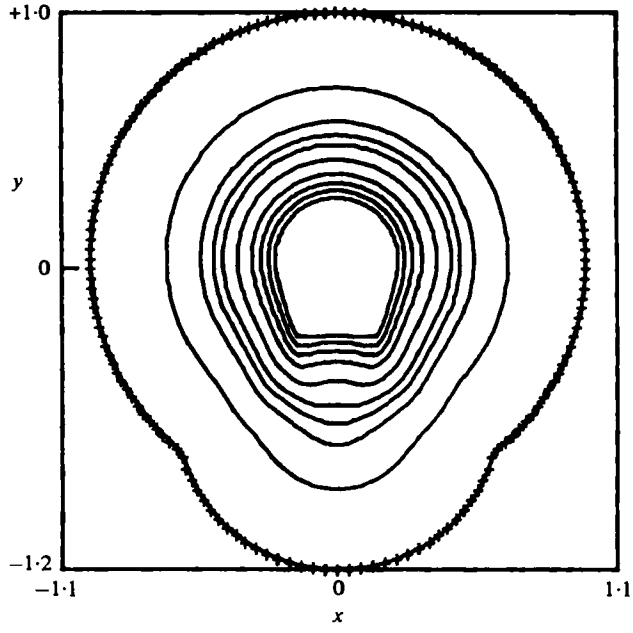

FIGURE 13. Example of an unstable spherical cap perturbation where kink instability forms after one oscillation. ($\alpha = 39°$, $\beta = 34°$, $\delta R/R = 0{\cdot}25$.)

exponent have been computed for the implosion problem (Yousaf 1974) and density variation problem (Yousaf 1977) where self-similar solutions are available, but have not yet been computed for the general problem of self-similar implosion into a medium with variable density.

The compatibility relation along the inward-directed characteristic is given by

$$dp + \rho a\, du + \frac{\rho a^2 d}{u+a}\frac{dA}{A} = 0, \tag{50}$$

while the Hugoniot relations behind a strong shock ($M \to \infty$) are given by

$$u = \frac{2}{\gamma+1}v, \quad p = \frac{2}{\gamma+1}\bar{\rho}v^2 = \bar{\rho}uv, \quad \rho = \frac{\gamma+1}{\gamma-1}\bar{\rho}, \quad a^2 = \frac{\gamma p}{\rho} = \frac{2\gamma(\gamma-1)}{(\gamma+1)^2}v^2, \tag{51}$$

where u is the fluid velocity behind the shock, p is the pressure behind the shock, ρ is the density behind the shock, and $\bar{\rho}$ is the undisturbed density. Differentiating the relation for p, we get

$$dp = \frac{2}{\gamma+1}v^2 d\bar{\rho} + \frac{4}{\gamma+1}\bar{\rho}v\, dv. \tag{52}$$

Combining equations (50)–(52), we have

$$\frac{2}{\gamma+1}v^2 d\bar{\rho} + \left[\frac{4}{\gamma+1} + \frac{2}{\gamma+1}\left(\frac{2\gamma}{\gamma-1}\right)^{\frac{1}{2}}\right]\bar{\rho}v\, dv + \frac{4\gamma}{\{2(\gamma+1)+[2(\gamma-1)]\}}\bar{\rho}v^2\frac{dA}{A}, \tag{53}$$

or

$$\frac{dv}{v} = -\left[\frac{\gamma+2}{\gamma} + \left(\frac{2\gamma}{\gamma-1}\right)^{\frac{1}{2}}\right]^{-1}\frac{dA}{A} - \left[2 + \left(\frac{2\gamma}{\gamma-1}\right)^{\frac{1}{2}}\right]^{-1}\frac{d\bar{\rho}}{\bar{\rho}}. \tag{54}$$

If we now write this in the form of (7) we have

$$\lambda(\dot{v}/v) = -\dot{A}/A - \kappa\dot{\bar{\rho}}/\bar{\rho}. \tag{55}$$

Using equations (4), (6) and (10) and the relation

$$\dot{\bar{\rho}} = \mathbf{v}.\nabla\bar{\rho}, \tag{56}$$

we have

$$(\lambda/v)^{\cdot} = \nabla.\mathbf{n} + \kappa\mathbf{n}.\nabla\ln\bar{\rho}. \tag{57}$$

Assuming a density profile of the form $\tilde{\rho} \sim r^{-q}$ the zeroth-order symmetric equation becomes similar to (15),

$$(\lambda/\dot{r})^{\cdot} = (\alpha - \kappa q)/r. \tag{58}$$

This has a solution analogous to (18),

$$r = R(\omega t)^{\lambda/(\lambda+\alpha-\kappa q)}. \tag{59}$$

The effect of a positive q (density increasing toward the axis) is to cause the shock to accelerate more slowly than the $q = 0$ case. (A negative q will cause the shock to accelerate faster.)

Again linearizing the equations as in § 2, we have to first order

$$\begin{aligned}(-\lambda v_1/v_0^2)^{\cdot} = \nabla_0.\mathbf{n}_1 - (\nabla_0\boldsymbol{\xi}) : (\nabla_0\mathbf{n}_0) + [\kappa\mathbf{n}_1.\nabla_0\ln\bar{\rho} \\ - \mathbf{n}_0.(\nabla\boldsymbol{\xi}).\nabla_0\ln\bar{\rho} + \mathbf{n}_0.\nabla_0(\boldsymbol{\xi}.\nabla_0)\ln\bar{\rho}].\end{aligned} \tag{60}$$

Using vector manipulations similar to those in § 2, we obtain

$$-(\lambda\mathbf{n}_0.\dot{\boldsymbol{\xi}}/v_0^2) = -\nabla_0.[(\mathbf{I} - \mathbf{n}_0\mathbf{n}_0).\nabla(\mathbf{n}_0.\boldsymbol{\xi})] + \boldsymbol{\xi}.\nabla_0(\alpha/r_0) + \mathbf{n}_0\boldsymbol{\xi} : \nabla_0\nabla_0\ln\bar{\rho}. \tag{61}$$

The last term of (61) adds an additional term to (29), given by

$$\mathbf{n}_0\boldsymbol{\xi} : \nabla_0\nabla_0\ln\bar{\rho} = \zeta(\ln\bar{\rho})'', \tag{62}$$

where the double prime indicates a derivative with respect to r_0. Thus equation (61) becomes

$$-(\lambda\dot{\zeta}/v_0^2)^{\cdot} = (Q - \alpha + \kappa q)\,\zeta/r_0^2. \tag{63}$$

Now from (53) we get

$$\frac{d\ln v_0}{dr_0} = -\frac{\alpha - \kappa q}{\lambda} r_0^{-1}, \tag{64}$$

and using (30) we have, after a little algebraic manipulation,

$$\lambda\frac{d^2\zeta}{dr_0^2} + \frac{\alpha - \kappa q}{r_0}\frac{d\zeta}{dr_0} + \frac{Q - \alpha + \kappa q}{r_0^2}\zeta = 0. \tag{65}$$

The resulting indicial equation is

$$\lambda\beta(\beta - 1) + (\alpha - \kappa q)\,\beta + (Q - \alpha + \kappa q) = 0, \tag{66}$$

or

$$\beta = \{\lambda - \alpha + \kappa q \pm [(\lambda + \alpha - \kappa q)^2 - 4\lambda Q]\}^{\frac{1}{2}}/2\lambda. \tag{67}$$

We note from this result that the effect of including density variation is found to first order by replacing everywhere the term α by $\alpha - \kappa q$. That is, the acceleration normally due to the geometric factor α is modified by an additional term κq related to the acceleration caused by a density variation. Positive q (density increasing toward

the axis) has the effect of reducing the acceleration due to geometric convergence. For sufficiently large q the acceleration vanishes. This situation, however, could lead to rather large errors if the wave system behind the shock were to catch up in violation of the CCW approximation. The ratio of the disturbance amplitude to the zeroth-order radius continues to satisfy $\zeta/r_0 \sim t^{-\frac{1}{2}}$, with the frequency appropriately modified. In terms of the zeroth-order radius, however, the growth becomes $\zeta/r_0 \sim r^{-(\lambda+\alpha-\kappa q)/(2\lambda)}$. A positive q thus decreases the relative growth of the shock perturbation as a function of the shock radius.

8. Conclusions

The CCW approximation, which appears to be very accurate for computing converging shock waves, predicts that the converging shock is always unstable, in the sense that the ratio of the perturbation size to the average radius diverges at the time of collapse. The cylindrical and spherical cases differ only quantitatively. The growth rate is only a power law, however, and therefore is not as serious as an exponential growth. For mode number greater than unity, the perturbations oscillate in $\ln t$ with a mode-number-dependent period. The amplitude growth, however, is independent of mode number.

For sufficiently large amplitude the linear behaviour breaks down and the solution develops nonlinearly into a kink form, where a reflected shock is left behind in the material, serving as a potential loss of shock energy in the collapsing shock.

We are grateful to one of the referees for providing us with a copy of Butler's stability calculations cited in § 3.

REFERENCES

BERNSTEIN, I. B. & BOOK, D. L. 1978 *Astrophys. J.* **225**, 633.

BUTLER, D. S. 1955 Symp. on Blast and Shock Waves. Fort Halstead, Kent, U.K.: Armament Research and Development Establishment, Ministry of Supply.

CHESTER, W. 1954 *Phil. Mag.* **45**, 1293.

CHISNELL, R. F. 1955 *Proc. R. Soc. Lond.* A **232**, 350.

FONG, K. & AHLBORN, B. 1979 *Phys. Fluids* **22**, 416.

GUDERLEY, G. 1942 *Luftfahrtforschung* **18**, 302.

HAYES, W. D. 1968 *J. Fluid Mech.* **32**, 317.

SAKURAI, A. 1960 *Comm. Pure Appl. Math.* **13**, 353.

WHITHAM, G. B. 1957 *J. Fluid Mech.* **2**, 146.

WHITHAM, G. B. 1958 *J. Fluid Mech.* **4**, 337.

WHITHAM, G. B. 1974 *Linear and Nonlinear Waves*, p. 309. Wiley.

YOUSAF, M. 1974 *J. Fluid Mech.* **66**, 577.

YOUSAF, M. 1977 *Phys. Fluids* **21**, 217.